Journal of Photochemistry & Photobiology, B: Biology 235 (2022) 112562

Contents lists available at ScienceDirect

Journal of Photochemistry & Photobiology, B: Biology

journal homepage: www.elsevier.com/locate/jphotobiol

Stimulated Raman generation of aqueous singlet oxygen without photosensitizers

Aristides Marcano Olaizola [a,*], Robinson Kuis [b], Anthony Johnson [b], David Kingsley [c]

[a] Division of Physics, Engineering, Mathematics, and Computer Science, Delaware State University, 1200 North DuPont Highway, Dover, DE 19901, USA
[b] Center for Advanced Studies in Photonics Research, University of Maryland Baltimore County, 1000 Hilltop Circle, Baltimore, MD 21250, United States of America
[c] Residue Chemistry and Predictive Microbiology Research Unit, US Dept. of Agriculture, Agriculture Research Service, Delaware State University, 1200 North DuPont Highway, Dover, DE 19901, United States of America

ARTICLE INFO

Keywords:
Singlet oxygen
Raman spectroscopy
Raman transitions

ABSTRACT

Singlet oxygen is traditionally produced via photosensitizer molecules such as methylene blue, which function as catalysts. Here we investigate stimulated Raman generation of singlet oxygen from dissolved oxygen in both water (H_2O) and heavy water (D_2O) using nanosecond-pulsed visible blue laser light in the 400–440 nm spectral region without singlet oxygen photosensitizers. We report an oxygen-dependent Stokes peak in the red spectrum (600–670 nm) that is identical when produced in H_2O and D_2O. These red Stokes photons are not detected when an oxygen quencher is present. Temporal photodepletion of the uric acid absorbance peak at 294 nm is consistent with singlet oxygen generation. We postulate that a two-photon stimulated Raman process produces singlet oxygen from O_2 dissolved within the solvents. We note that the energy difference between input and output photons of 0.97 eV is precisely the energy needed to excite O_2 to its singlet state.

1. Introduction

Singlet oxygen $O_2(^1\Delta_g)$ is the oxygen molecule at its lowest excited electronic state. The molecule is highly electrophilic, readily causing electron couples from covalent bonds of complex molecules to break apart. Researchers have used the $O_2(^1\Delta_g)$ in photo-inactivation of viruses, fungi, and bacteria [1–6], photodynamic treatments of cancer [7–9], photo-disinfections of blood and pharmaceutical products [10,11], protein activity research [12,13], environmental water studies [14–17], photochemical reactions [18], and in other significant applications. The generally accepted dogma to produce the $O_2(^1\Delta_g)$ level consists of an indirect transition based on photosensitizers [19–22]. Photosensitizers are large molecules with large numbers of π bonds that facilitate the absorption of visible light energy. The absorbed photon energy accumulates in the photosensitizers' metastable triplet state, enabling energy transmission to the molecular oxygen via collisional relaxation to transition toward the $O_2(^1\Delta_g)$ state.

Several authors have experimentally-produced direct singlet photon photoactivation of molecular oxygen without photosensitizers using infrared radiation at 765, 1268, and 1064 nm [23–28]. However, the authors reported limited quantum efficiency. Presumably these results are consistent with quantum mechanics, which predicts low probabilities for the direct one-photon dipolar transition from the ground state toward the $O_2(^1\Delta_g)$ state. The transition violates the spin, orbital, and wave-function symmetry selection rules, making the direct excitation highly improbable. Bregnhøj and Ogilby have noted two-photon excitation to produce $O_2(^1\Delta_g)$ in aerated solvents without using photosensitizers [29]. The aeration gives rise to a UV absorbing band associated with transitioning from a ground state oxygen-solvent to an oxygen-solvent charge-transfer (CT) state [30–32]. The band can be excited via a two-photon process using visible light. The CT state decays radiation-less, producing a significant amount of $O_2(^1\Delta_g)$. Bregnhøj and Ogilby also provide evidence for a long-lived photo-produced species in liquid water that may sensitize the $O_2(^1\Delta_g)$ production [29]. However, this path of $O_2(^1\Delta_g)$ photoproduction does not generate additional luminescence as it is the case in the Raman photo-excitation we discuss here.

In previous work, we proposed an alternative path for photosensitizer-free $O_2(^1\Delta_g)$ excitation by visible blue light based on stimulated Raman scattering [33]. Here we provide experimental evidences to support the Raman hypothesis by irradiating distilled water (H_2O) and heavy water (D_2O) using nanosecond pulses of light in the blue spectral region. Raman is fundamentally a two-photon process, where incoming (pump) photons generate outgoing (Stokes) photons of

* Corresponding author.
E-mail address: amarcano@desu.edu (A.M. Olaizola).

https://doi.org/10.1016/j.jphotobiol.2022.112562
Received 24 May 2022; Received in revised form 23 August 2022; Accepted 1 September 2022
Available online 8 September 2022

less energy. The difference in energy matches the energy needed to excite the oxygen molecule. Quantum mechanics theory does permit a high probability Raman transition wherever the one-photon dipolar excitation is not predicted. When irradiating with blue light (410–440 nm), the Raman interaction should produce a Stokes photon in the red region of the spectra (600–670 nm). The energy difference between the incoming and Stokes photons is 0.97 eV, which corresponds to the energy gap between the ground and the $O_2(^1\Delta_g)$ level. Thus, the Raman method provides a Stokes signal that perfectly corresponds to the oxygen excitation toward its $O_2(^1\Delta_g)$ state.

The two-photon process exciting the CT states discussed above may be a competing path for $O_2(^1\Delta_g)$ photoproduction. Relaxation from the CT state toward the $O_2(^1\Delta_g)$ level is radiation-less. Thus, it does not contribute to the Stokes peak observed in the Raman experiments. However, any interaction of the oxygen molecule with its surrounding solvent molecules is expected to significantly affect the Stokes response's spectral width.

The $O_2(^1\Delta_g)$ Raman photogeneration using blue light is consistent with our previous finding of photosensitizer-free photoinactivation of viruses using CW and femtosecond light of similar wavelengths, demonstrating the potential photobiology applications of the results [34].

2. Theoretical Considerations

Fig. 1 shows a simplified schematic of the lowest electronic level of the oxygen molecule. The $O_2(^1\Delta_g)$ level is at 0.97 eV from the ground state $O_2(^3\Sigma_g^-)$. Each level exhibits a complex vibrational-rotational structure represented by the multiple solid lines. The gap corresponds to the energy of a photon of wavelength 1269 nm. A pumping photon at 410 nm provides an energy of 3.03 eV. By generating a Stokes photon of 2.06 eV, the Raman transition excites the $O_2(^1\Delta_g)$ state. The dashed line in Fig. 1 represents a virtual state corresponding to the two-photon Raman transition. We estimate the minimal wavelength of the required Stokes photon λ_s using the equation.

$$1/\lambda_s \leq 1/(410\ \text{nm}) - 1/(1269\ \text{nm}) \quad (1)$$

We obtain $\lambda_s \geq 605\ nm$. Each of the vibrational-rotational sublevels may contribute to the total Raman signal. For example, the second vibrational level $O_2(^1\Delta_g)(\nu = 1)$ corresponds to a transition wavelength of 1065 nm [35]. When pumping at 410 nm, the resulting Stokes signal is at 666 nm. Thus, the combined $O_2(^1\Delta_g)$ Stokes signal may exhibit a full-width-half-maximum (FWHM) of tens of nanometers in the red spectral region. Each line is also broadened because of the interaction between the dissolved oxygen and the surrounding solvent molecule. Wessels and Rodgers studied the spectral properties of the luminescence line $O_2(^1\Delta_g) \rightarrow O_2(^3\Sigma_g^-)$ in many solvents [36]. They report on spectral line's broadening and peak shifts. They found a linear correspondence between solvent's polarizability and the peak position in most of the solvents. The formation of complex solute-solvent structures, including oxygen-solvent CT states may contribute to the broadening. Macpherson and Truscott also reported broadening and spectral shift of the $O_2(^1\Delta_g)$ phosphorescence in different solvents [37]. The authors attributed the observed spectral broadening to van der Walls complexes of $O_2(^1\Delta_g)$ molecules with four to six solvent molecules or the repulsive long-range forces in perfluorocarbons solvents. They also studied correlations between the solvent polarizabilities and spectral shift and broadening of the $O_2(^1\Delta_g) \rightarrow O_2(^3\Sigma_g^-)$ line. The luminescence transition occurs between the lowest vibrational $O_2(^1\Delta_g)(0)$ sublevel and the ground state $O_2(^3\Sigma_g^-)$. The Raman line of the same transition is expected to be wider because it will include contributions from the lowest level and the rest of the sublevels of the $O_2(^1\Delta_g)$ electronic state. The nonlinear character of the stimulated Raman generation can also affect the spectral properties of the Stokes line. A detailed study of these effects falls out of the scope of the present work.

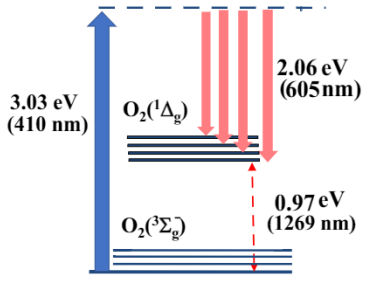

Fig. 1. Schematic of the excitation of the a $O_2(^1\Delta_g)$ state. The pumping photon at 410 nm generates the Stokes photon with a minimal wavelength 605 nm resulting in the transition to bottom of the $O_2(^1\Delta_g)$ level.

Raman is generally applied to study transitions between molecular vibrational-rotational states. However, Raman transitions between electronic states have also been reported in the past [38–40]. For the $O_2(^1\Delta_g)$ electronic state excitation, the two-photon Raman transition is expected to occur considering the "golden rule" of spectroscopy which predicts a high-probable Raman transition wherever the direct excitation is not allowed by Quantum Mechanics selection rules.

3. Methods

Here, we describe a stimulated Raman excitation of oxygen dissolved in H_2O and D_2O at room temperature and one-atmosphere pressure using nanosecond pulses from an optical parametric oscillator (OPO). The experiments identify peaks that represent the contribution from the stretching modes of the solvent molecules and, most importantly, a smaller red spectrum peak that we identify as the Raman response of $O_2(^1\Delta_g)$ oxygen molecules dissolved in the samples.

Fig. 2 shows a schematic of the Raman experiment. The pump source was an optical parametric oscillator (OPO Radiant QX 4130, OPOTEK) tunable in the visible region (410–700 nm). In the device, an Nd-YAG laser at 1064 pumps the OPO crystal. The system generated 10-ns pulses at a 10 Hz rate. The average energy per pulse was about 30 mJ. OPO radiation was used at 410, 420, 430, and 440 nm. A beam-splitter (B) redirected a small portion of the light to a reference detector (Ref). A 40-cm focal length lens (L_1) focused the OPO light onto the sample.

The samples were doubled-distilled H_2O and D_2O (99.9 atom % D, Sigma Aldrich) in 30-cm and 10-cm length glass cuvettes. The long-pass cuvette had two purposes. First, to provide enough path length of the sample, and second, to avoid damage to the cuvette's windows, ensuring that the light intensity at the entrance and exit of the cuvette is small enough. The focused light stimulated Raman signals in slightly different directions than the original pumping beam. Most of the light was in the beam center, which also contains the pumping light. The stimulated Raman also generated a ring of light centered in the direction of the original pumping beam. A blocker (D) was used to eliminate the beam's central spot. The procedure depleted most of the pumping light. A long-pass filter (LPF) blocked the remnant excitation light. Lens L_2 collimated the light from the ring. A mirror (M) redirected part of the light of the ring structure into a monochromator (Cornerstone 260, Newport).

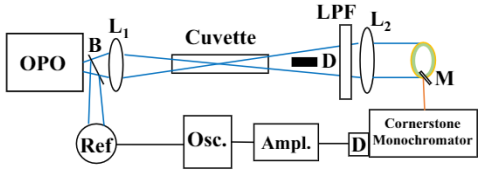

Fig. 2. Raman scattering experimental set-up consisting of an optical parametric oscillator (OPO), a beam splitter (B), a reference diode detector (Ref), a focusing lens (L_1), a long-path glass cuvette, a beam blocker (D), a long-pass filter (LPF), a collimating lens (L_2), a mirror, a monochromator, a current amplifier and a digital oscilloscope (Osc).

Rotation of the mirror allowed the selection of different parts of the ring structure. A diode detector (DET36A2, Thorlabs) collected the light from the monochromator sending the generated signal toward a current pre-amplifier (SR570 Stanford Research). The amplified signal was redirected to a digital oscilloscope (TDS3052, Tektronix) for averaging and recording.

We used a glass filter blocking all light with wavelengths below 590 nm to monitor the suspected $O_2(^1\Delta_g)$ Stokes peak in the spectrum's red region. The filter depleted the contributions from the stretching modes of the solvent molecules. To demonstrate that the observed "red peak" is oxygen-related, we reduced the oxygen concentration in the solvents by adding the oxygen quencher sodium bisulfite ($NaHSO_3$, Sigma Aldrich). We also monitored the "red peak" decreasing after purging the sample with argon for a few hours. We used the Optical DO sensor (Vernier) to determine the O_2 concentration in the samples.

We have also measured the "red peak" in different solvents (methanol, glycerol, and hexane) to demonstrate that its presence is related to the dissolved O_2 and not to the nature of the solvent.

We measured the UV spectra of irradiated diluted solutions (0.1 mM) of uric acid ($C_5H_4N_4O_3$, 99% Alfa Aesar) in H_2O and D_2O using a UV-VI-NIR spectrophotometer (Evolution 201, Thermo Scientific). We measured the spectra between 190 and 400 nm. We used standard 1-cm pathlength spectroscopic quartz cells that contained about 3 ml of the irradiated samples. The spectra of uric acid solutions with $NaHSO_3$ at 2.4 and 6.4 mg/ml concentrations were measured.

4. Results and Analysis

Fig. 3-left shows the stimulated Raman spectra collected for H_2O (open blue squares) and D_2O (open red stars) when pumping at 410 nm. Fig. 3-right exhibits the spectra obtained when pumping at 440 nm. We observed two peaks shifting according to the pumping wavelength changes, confirming their Raman character. The first Stokes peak for H_2O occurs at 475 nm and 515 nm when pumping at 410 nm and 440 nm. The corresponding peaks for D_2O occur at 454 nm and 492 nm, respectively. The Stokes frequency shift of the first peak averages (3340 $\pm$ 20) cm^{-1} for H_2O and (2250 $\pm$ 20) cm^{-1} for D_2O. The values of both solvent molecules agree well with reported stretching mode frequencies [41–43]. The H_2O's second peak occurs at 567 nm and 630 nm when pumping at 410 nm and 440 nm light. We observe similar additional peaks for D_2O at 507 nm and 556 nm, respectively, when pumping with 410 and 440 nm light. The frequency shifts of the second peak average (6743 $\pm$ 110) cm^{-1} and (4770 $\pm$ 60) cm^{-1} for H_2O and D_2O.

Because the value of the second peak is near twice the shift of the first peak, we interpret the signal as resulting from a second-order cascade Raman effect with the Stokes light corresponding to the first peak that produces this secondary Raman emission. A recent publication describes this Raman cascade effect in D_2O [41].

In contrast to other observed peaks, a third "red peak," indicated by the green star, exhibits the same shape and frequency shift for H_2O and D_2O and is much broader than the previous peaks. For both solvents, peak detection occurs at (600 $\pm$ 25) nm and (670 $\pm$ 25) nm when pumping at 410 nm and 440 nm, respectively. This frequency shift is (7856 $\pm$ 240) cm^{-1} and does not coincide with possible water molecule vibrations [41–43]. The Stokes frequency shift of the "red peak" in both solvents corresponds to the energy of (0.97 $\pm$ 0.3) eV in agreement with the transition to the $O_2(^1\Delta_g)$ level. We interpret the third "red peak" as generated from the oxygen molecules dissolved within the water. The corresponding wavelength is (1272 $\pm$ 44) nm, which agrees with the predicted $O_2(^1\Delta_g)$ phosphorescence photoemission [44–46]. Experiments pumping at 420 nm and 430 nm are consistent with those observed at 410 and 440 nm, with the first two shifted peaks present and a solvent-independent "red peak" with H_2O and D_2O.

We measure an average FWHM of 3 nm and 7 nm for the first and the second-order Stokes signals corresponding to the solvent stretching mode, respectively. This FWHM is smaller than that of the infrared absorption spectra because of the stimulated Raman character of the lines. The effect has been reported elsewhere [41–43]. For the "red peak," we estimate an FWHM of 25 nm. The observed differences confirm the different physical origins of the peaks. The Raman transition generating the solvent signals occurs between vibrational levels. The two-photon $O_2(^1\Delta_g)$ Raman transition occurs between electronic states, which exhibit a structure more complex than the individual vibrational levels.

Krasnovsky and Ambartzumian measured an FWHM of 18 nm for the $O_2(^1\Delta_g)$ phosphorescence peak in tetracene [45]. A recent communication reports an FWHM of 7 nm for the transition from the ground state $[O_2(3\Sigma_g^-]$ toward to second excited electronic level of oxygen $[O_2(^1\Sigma_g^+)]$ at 765 nm in toluene [46]. Our experiments confirm that the stimulated Raman process generating the "red peak" exhibits a spectral response broader than the one-photon luminescence transitions of the excited oxygen molecule. As discussed above, the Raman transition is a two-photon interaction where different levels (rotational-vibrational) of the electronic band corresponding to the $O_2(^1\Delta_g)$ state may contribute (see discussion of Fig. 1). Interaction with the surrounding solvent molecules broadens the contributions of individual levels [36,37,44]. As a result, the Stokes line of the electronic state appears heavily broadened. The spectral properties of the $O_2(^1\Delta_g)$ NIR phosphorescence are different. As discussed above, this one-photon transition occurs from the bottom of the $O_2(^1\Delta_g)$ electronic level toward the ground level. The other sub-levels of the $O_2(^1\Delta_g)$ electronic state above the bottom do not contribute to the one-photon luminescence.

To further test that the red region's peaks are oxygen-dependent, we use H_2O solutions of sodium bisulfite ($NaHSO_3$). Sodium bisulfite is a well-known oxygen quencher [47]. We use a long-pass filter blocking any light below 590 nm to deplete the Stokes peaks from the stretching modes. Fig. 4-left shows the Stokes peaks in the red region for H_2O (blue line) and solutions of sodium bisulfite ($NaHSO_3$) in H_2O at concentrations of 40 mg/ml (red line). The solution with $NaHSO_3$ exhibits a significantly reduced "red peak." Fig. 4-right shows similar results for the solution of $NaHSO_3$ in D_2O. The oxygen quencher depletes the oxygen concentration, reducing the "red peak." We measured an oxygen concentration of 0.01 mg/L after the procedure, corresponding to the sensor's minimal resolution.

As additional evidence, we measure the temporal destruction of uric

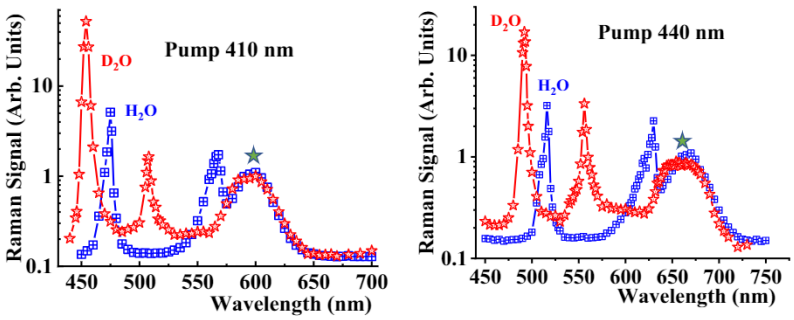

Fig. 3. Left -Stokes peaks of the Raman spectra from water (blue crossed squares) and heavy water (open red stars) when pumping at 410 nm. The first two peaks correspond to the stretching modes of the solvent molecule (H_2O or D_2O). The third peak, indicated by the green star, is associated with the generation of the $O_2(^1\Delta_g)$ state. Right - Stokes peaks of the Raman spectra from water (blue crossed squares) and heavy water (open red stars) when pumping at 440 nm. The first two peaks correspond to the stretching modes of the solvent molecules. The third peak, indicated by the green star, is associated with the generation of the $O_2(^1\Delta_g)$ state. (For interpretation of the references to colour in this figure legend, the reader is referred to the web version of this article.)

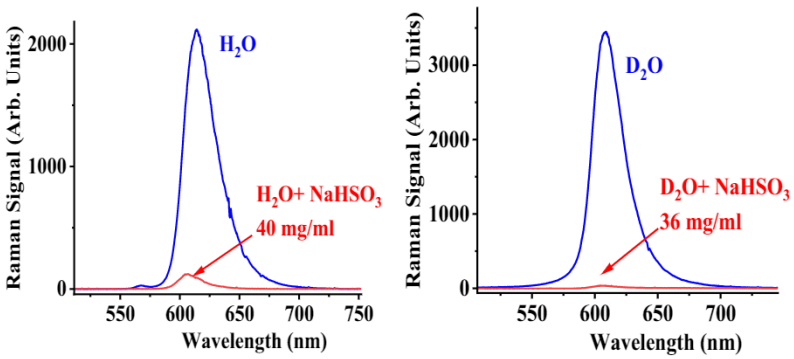

Fig. 4. Left - Stokes red peak in H_2O obtained using a long-pass filter >590 nm in front of the monochromator (blue line) when pumping at 410 nm. When adding the oxygen quencher $NaHSO_3$ at a 40 mg/ml concentration, the peak substantially decreases. Right - The same Stokes red peak measured in D_2O. Again, the addition of $NaHSO_3$ depletes the signal. (For interpretation of the references to colour in this figure legend, the reader is referred to the web version of this article.)

acid as a measure of $O_2(^1\Delta_g)$ production. We determine the UV spectrum of a diluted uric acid solution in distilled water irradiated at 410 nm at different exposure times. The UV absorbance peak at 294 nm exhibits photodepletion upon irradiation due to a lytic reaction between the $O_2(^1\Delta_g)$ and uric acid molecules [48,49]. After irradiation, we measure the corresponding UV spectra. Fig. 5-left shows the UV spectra of a 0.1 mM uric acid solution in H_2O. The non-irradiated sample has a clear peak at 294 nm (black line). The peak consistently decreases upon irradiation over one hour (red line), two hours (blue line), and three hours (green line). As generally accepted, this indicates that $O_2(^1\Delta_g)$ is being produced [48,49].

We have also used uric acid solutions in D_2O, yielding similar results. Adding the oxygen quencher $NaHSO_3$ to the solution substantially reduces the photobleaching of the uric acid UV peak. Fig. 5-right shows the UV spectra of a 0.1 mM uric acid water solution with $NaHSO_3$ added at a 6.4 mg/ml concentration. Irradiating by a 410 nm laser light for one hour (red line), two hours (blue line), and four hours (olive line) does not significantly affect the signal. We observe peak reductions of <4%, confirming that the destruction of uric acid is oxygen-dependent. We previously reported on aerated and non-aerated experiments using the uric acid $O_2(^1\Delta_g)$ sensor [33]. The aeration was performed by bubbling air through the sample for over 30 min. Bubbling nitrogen provided the conditions with reduced oxygen present in the solvent. This last sample did not show the depletion of the uric acid UV peak upon irradiation, confirming the uric acid method's ability as an $O_2(^1\Delta_g)$ sensor.

As additional evidence that we are generating $O_2(^1\Delta_g)$, we have also completed the purging of H_2O samples with argon. Fig. 6-left shows the "red peak" before the purging procedure (red line) when pumping at 410 nm. We detected an initial O_2 concentration of 8.5 mg/L in the sample. After purging for three hours using argon, we reduced the O_2 concentration to 1 mg/L. Correspondingly, the purging reduces the "red peak" by more than four times (blue line).

We have discussed Raman experiments in H_2O and D_2O. Similar Raman studies can be performed in other solvents. However, the presence of solvent strong stretching Raman modes, which may coincide with the $O_2(^1\Delta_g)$ Stokes line, complicates the analysis. We have measured the "red peak" for different solvents. Some solvents like methanol exhibit additional stretching mode peaks that superimpose over the "red peak," making the interpretation difficult. However, we noted that the power dependence of the solvent stretching modes and the "red peak" are different. We managed to reduce the stretching mode effects by decreasing the laser intensity. Fig. 6-right shows production of the "red peak' within water (red line), methanol (black line), glycerol (blue line), and hexane (green line) when pumping at 410 nm. The position of the "red peak" shifts slightly, and its FWHM changes. As discussed above, Different groups studied the solvent's effects on the $O_2(^1\Delta_g)$ phosphorescence line [36,37]. They reported similar effects, which they associate with forming van der Waals complexes of $O_2(^1\Delta_g)$ with solvents molecules and other phenomena. The stimulated Raman peak from $O_2(^1\Delta_g)$ provides an alternative way to study the interaction with the surrounding solvent molecules.

Detection of the NIR spectra around 1269 nm is proof of $O_2(^1\Delta_g)$ photogeneration [50]. The $O_2(^1\Delta_g)$ molecule relaxes toward the ground, emitting this particular NIR wavelength. However, the signal is generally weak because of the forbidden character of the transition. We were unable to resolve any phosphorescence emission from D_2O or H_2O in the conditions of our experiments, presumably because of the low phosphorescence yields in the solvents.

Despite the lack of phosphorescence confirmation, we have seven observations that support the Raman hypothesis of $O_2(^1\Delta_g)$ generation. 1) The frequency shifts of the red Stokes peaks correspond to the energy of the $O_2(^1\Delta_g)$ level. 2) The "red peak" position is not influenced by the solvent, H_2O, or D_2O, indicating that the solvent vibrational modes do not generate this peak. 3) The "red peak" is depleted when an oxygen quencher (sodium bisulfite) is added to the solvents. 4) The photodepletion of the UV peak of uric acid upon illumination with blue light provides direct evidence for an $O_2(^1\Delta_g)$ generation. 5) The reduction of the photobleaching of the UV uric acid peak when an oxygen quencher is added. 6) The reduction of the red peak when reducing the oxygen concentration after purging the sample using argon. 7) The observation

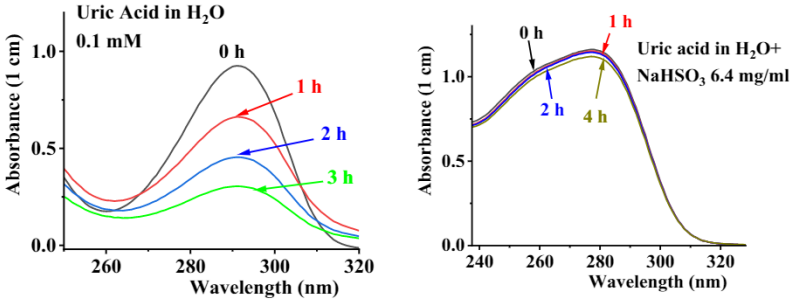

Fig. 5. Left - UV peak at 294 nm of a 0.1 mM uric acid water solution before irradiation (black line). Irradiation of the sample for one-hour (red line), two hours (blue line), and three hours induces the photobleaching of the peak as evidence of $O_2(^1\Delta_g)$ generation. Right - The same 294 nm peak of the uric acid water solution when adding the oxygen quencher $NaHSO_3$. Almost no photobleaching is observed due to the depleted oxygen concentration in the solvent. (For interpretation of the references to colour in this figure legend, the reader is referred to the web version of this article.)

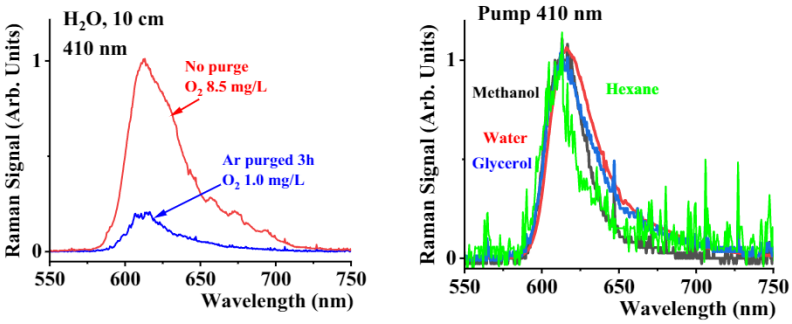

Fig. 6. Left - The "red peak" in water with an initial oxygen concentration of 8.5 mg/L (red line). The blue line shows the same red peak after purging the sample for three hours with argon reducing the oxygen concentration to 1 mg/L. Right – The "red peak" measured for different solvents: H_2O (red line), methanol (black line), glycerol (blue line), and hexane (green line). (For interpretation of the references to colour in this figure legend, the reader is referred to the web version of this article.)

of the "red peak" in different solvents. Furthermore, when tuning the pumping light from 410 to 440 nm, all observed "red peaks" shift as expected for a Stokes signal, as do the solvent stretching vibration peaks. The solvent stretching peaks confirms a stimulated Raman coherent interaction and validates instrument calibration. Viewing our results within the context of reactive oxygen theory, as shown in Fig. 1, we see that 410–440 nm light provides sufficient energy (3.03–2.8 eV) to generate an $O_2(^1\Delta_g)$ state by releasing 2.06–1.91 eV (605–670 nm Stokes light) followed by a transition from ground to the $O_2(^1\Delta_g)$ state. The difference between the energies of both the pump and Stokes photons is 0.97 eV, which corresponds to the energy needed for $O_2(^1\Delta_g)$ excitation.

Studies on an $O_2(^1\Delta_g)$ chemiluminescence have discussed the fact that the $O_2(^1\Delta_g)$ molecule can form a dimeric aggregate that relaxes emitting photons in the red (633 nm) and infrared (703 nm) regions (dimol emission) [51]. This signal may overlap with the observed Stokes peak in the red spectral region. However, the Stokes signal wavelength depends on the pumping wavelength, as shown in Fig. 3. This property helps isolate the Raman response from other $O_2(^1\Delta_g)$ chemiluminescence contributions.

Our experiments could not detect the $O_2(^1\Delta_g)$ transition anti-Stokes component. When pumping in the blue region (410–440 nm), the $O_2(^1\Delta_g)$ anti-Stokes components should be in the UV region 309–325 nm. We note that the H_2O absorption in the 300–320 region (0.03 m^{-1}) is about ten times larger than the absorption at 410 nm (0.003–0.004 m^{-1}) [52,53], making it more challenging to produce the stimulated anti-Stokes components for the power levels used in the experiments.

This work demonstrated the Raman path for $O_2(^1\Delta_g)$ photoexcitation using visible light in a photosensitizer-free environment. We have not compared the Raman approach with the photosensitized method nor estimated the quantum yield of $O_2(^1\Delta_g)$ generation. However, the general theory of the stimulated Raman effect shows that Stokes signals exhibit an intrinsic exponential growth (Raman gain) with the intensity of the pumping light, the path-length of the interaction, the concentration of active molecules, and the probability of the Raman transition. This property has been well applied in developing Raman fiber lasers and high-sensitivity Raman sensors based on the Raman gain principle [54–56]. We predict that a significant $O_2(^1\Delta_g)$ quantum yield is reachable using this intrinsic property of the Raman approach.

We have also focused our study on pure solvents, not considering its possible applications to the biologically relevant system. Other effects may occur when using nanosecond high-intensity pulses in bio-tissue, like heating, nonlinear absorption, optoacoustic response, scattering, or other phenomena. The stimulated Raman excitation will compete for energy with these other effects. By carefully choosing the wavelength, duration, and power levels for each particular bio-system application, the stimulated Raman effect will still play a significant role.

5. Conclusions

We have completed a study of the Raman response of H_2O and D_2O upon nanosecond illumination in the blue region of the spectrum 410–440 nm. We report evidence of $O_2(^1\Delta_g)$ formation within aqueous solvents in the absence of photosensitizers based on peaks in the 600–660 nm region, which we postulate correspond to the Raman transition of ground oxygen dissolved in the solvents to generate the $O_2(^1\Delta_g)$ state. Experiments using sodium bisulfite as an oxygen quencher and UV spectroscopy of uric acid solutions confirm the $O_2(^1\Delta_g)$ generation.

Authors Contributions

A.M.O. proposed and conducted the experiments and data analysis. He also built and tested the experimental set-up, prepared the initial and final draft of the manuscript, and participated in discussions with the rest of the authors. D.K. proposed ideas and experiments, particularly with oxygen quenchers and uric acid measurements. He participated in the discussions and review of the manuscript. R.K. and A.J. participated equally in the discussion of the experimental results and review of the manuscript.

Additional Information

Correspondence and request for materials should be addressed to Aristides Marcano Olaizola.

Mention of trade names or commercial products is solely for the purpose of providing specific information and does not imply the recommendation or endorsement by the U.S. Department of Agriculture. USDA is an equal opportunity employer.

Author Statement

- We declare that any financial or non-financial assistance was not provided by a third party to complete this work.
- We declare no financial interest or relationship — *within the last 3 years* — related to the subject matter but not directly to this manuscript.
- We do not have patents or copyrights an author may have that are relevant to the work in the manuscript.
- We have no other activities to declare.

Declaration of Competing Interest

The authors declare the following financial interests/personal relationships which may be considered as potential competing interests:

No other activities.

Acknowledgements

We acknowledge the US National Science Foundation (Award 1831332) and the US Department of Defense (DOD Application No. 78038-RT-REP).

References

[1] L. Sobotta, P. Skupin-Mrugalska, J. Mielcarek, T. Goslinski, J. Balzarini, Photosensitizers mediated photodynamic inactivation against virus particles, Mini-Rev. Med. Chem. 15 (6) (2015) 503–521.

[2] L. Costa, M.A. Faustino, M.G. Neves, A. Cunha, A. Almeida, Photodynamic inactivation of mammalian viruses and bacteriophages, Viruses 4 (2012) 1034–1074.

[3] A. Wiehe, J.M. O'Brien, M.O. Senge, Trends and targets in antiviral phototherapy, Photochem. Photobiol. Sci. 18 (11) (2019) 2565–2612, https://doi.org/10.1039/c9pp00211a.

[4] M. Wainwright, Photoinactivation of viruses, Photochem. Photobiol. Sci. 3 (5) (2004) 406–411, https://doi.org/10.1039/b311903n.

[5] X.-J. Fu, Y.-Q. Zhu, Y.-B. Peng, Y.-S. Chen, Y.-P. Hu, H.-X. Lu, W.-R. Yu, Y. Fang, J.-Z. Du, M. Yao, Enzyme activated photodynamic therapy for methicillin-resistant *Staphylococcus aureus* infection both *in vitro* and *in vivo*, J. Photochem. Photobiol. B 136 (2014) 72–80, https://doi.org/10.1016/j.jphotobiol.2014.04.016.

[6] G. Jori, O. Coppellotti, Inactivation of pathogenic microorganisms by photodynamic techniques: mechanistic aspects and perspective applications, anti-infect, Agents Med. Chem. 6 (2007) 119–131.

[7] T.J. Dougherty, C.J. Gomer, B.W. Henderson, G. Jori, D. Kessel, M. Korbelik, J. Moan, Q. Peng, Photodynamic therapy, J. Natl. Cancer Inst. 90 (12) (1998) 889–905, https://doi.org/10.1093/jnci/90.12.889.

[8] M. Ochsner, Photodynamic therapy: the clinical perspective. Review on applications for control of diverse tumorous and non-tumorous diseases, Arzneimittelforschung 47 (11) (1997) 1185–1194.

[9] J.A. Carruth, Clinical applications of photodynamic therapy, Int. J. Clin. Pract. 52 (1) (1998) 39–42.

[10] S.J. Wagner, A. Skripchenko, Investigation of photosensitizing dyes for pathogen reduction in red cell suspensions, Biotech. Histochem. 78 (3–4) (2003) 171–177.

[11] H. Mohr, Virus inactivation of blood products by phenothiazine and light, Photochem. Photobiol. 65 (3) (1997) 441–445.

[12] A.E. Beermann, D.G. Jay, Chromophore-assisted laser inactivation of cellular proteins, Methods Cell Biol. 44 (1994) 715–732, https://doi.org/10.1016/s0091-679x(08)60940-1.

[13] D.G. Jay, Selective destruction of protein function by chromophore-assisted laser inactivation, Proc. Natl. Acad. Sci. U. S. A. 85 (1988) 5454–5458.

[14] F. Amat-Guerri, N.A. Garcia, Photodegradation of hydroxylated *N*-heteroaromatic derivatives in natural-like aquatic environments: a review of kinetic data of pesticide model compounds, Chemosphere 59 (2005) 1067–1082.

[15] C.K. Remucal, The role of indirect photochemical degradation in the environmental fate of pesticides: a review, Environ Sci Process Impacts 16 (4) (2014) 628–653.

[16] M. Ishihara, S. Fujisawa, Review. Photooxygenation, photodegradation and antioxidative activity of platonin, a cyanine photosensitizing dye, In Vivo 21 (2) (2007) 163–173.

[17] W.J. Cooper, R.G. Zika, Photochemical formation of hydrogen peroxide in surface and ground waters exposed to sunlight, Science 220 (1983) 711–712.

[18] M.A. Corsello, N.K. Garg, Synthetic chemistry fuels interdisciplinary approaches to the production of artemisinin, Nat. Prod. Rep. 32 (2015) 359–366.

[19] B.I. Kruft, A. Greer, Photosensitization reactions *in vitro* and *in vivo*, Photochem. Photobiol. 87 (2011) 1204–1213.

[20] A.A. Krasnovsky, Primary mechanisms of photoactivation of molecular oxygen. History of development and the modern status of research, Biochemistry 72 (2007) 1065–1080.

[21] J. Moan, P. Juzenas, Singlet oxygen in photosensitization, J. Environ. Pathol. Toxicol. Oncol. 25 (2006) 29–50.

[22] H.L. Clennan, New mechanistic and synthetic aspects of singlet oxygen chemistry, Tetrahedron 56 (2000) 9151–9179.

[23] A. Blázquez-Castro, Direct $^1O_2$ optical excitation: a tool for redox biology, Redox Biol. 13 (2017) 39–59, https://doi.org/10.1016/j.redox.2017.05.011.

[24] J.M. Bregnhøj, A. Blázquez-Castro, M. Westberg, T. Breitenbach, P.R. Ogilby, Direct 765 nm optical excitation of molecular oxygen in solution and in single mammalian cells, Phys. Chem. B 119 (17) (2015) 5422–5429, https://doi.org/10.1016/j.redox.2017.05.011.

[25] F. Anquez, P. Suret, S. Randoux, E. Courtade, El Yazidi Belkoura, Cell death induced by direct laser activation of singlet oxygen at 1270 nm, Laser Phys. 23 (2) (2013), 025601.

[26] S.G. Sokolovski, S.A. Zolotovskaya, A. Goltsov, C. Pourreyron, A.P. South, E. U. Rafailov, Infrared laser pulse triggers increased singlet oxygen production in tumour cells, Sci. Rep. 3 (2013) 3484, https://doi.org/10.1038/srep03484.

[27] A.A. Krasnovsky Jr., A.S. Kozlov, Ya.V. Roumbal, Photochemical investigation of the IR absorption bands of molecular oxygen in organic and aqueous environment, Photochem. Photobiol. Sci. 11 (2012) 988–997.

[28] M. P. Landry, P. M. McCall, Z. Qi, Y. R. Chemla. Characterization of photoactivated singlet oxygen damage in single-molecule optical trap experiments, Biophys. J., 2009; 97(8) (2009), pp. 2128–36. doi:https://doi.org/10.1016/j.bpj.2009.07.048.

[29] M. Bregnhøj, P. Ogilby, Two-photon excitation of neat aerated solvents with visible light produces singlet oxygen, J. Phys. Chem. A 123 (2019) 7567–7575.

[30] H. Tsubomura, R.S. Mulliken, Molecular complexes and their spectra XII. Ultraviolet absorption spectra caused by the interaction of oxygen with organic molecules, J. Am. Chem. Soc. 82 (1960) 5966–5974.

[31] P.-G. Jensen, J. Arnbjerg, L.P. Tolbod, R. Toftegaard, P.R. Ogilby, Influence of an intermolecular charge-transfer state on excited-state relaxation dynamics: solvents effect on the methylnaphthalene-oxygen system and its significance for singlet oxygen production, J. Phys. Chem. A 113 (2009) 9965–9973.

[32] C. Schweitzer, R. Schmidt, Physical mechanisms of generation and deactivation of singlet oxygen, Chem. Rev. 103 (2003) 1685–1758.

[33] A. Marcano Olaizola, J. Dorsett, D. Kingsley, R. Kuis, and A. Johnson. Blue-laser enhancer-free singlet oxygen generation in water and heavy water, Conference on Lasers and Electro-Optics, OSA Technical Digest (Optical Society of America, 2020), paper JTu2B.3.

[34] D.H. Kingsley, R. Kuis, R. Perez, I. Basaldua, P. Burkins, A. Marcano, A. Johnson, Oxygen-dependent laser inactivation of murine norovirus using visible light lasers, Virol. J. 15 (2018) 117–124, https://doi.org/10.1038/srep0348410.1186/s12985-018-1019-2.

[35] R.M. Badger, A.C. Wright, R.F. Whitlock, Absolute intensities of the discrete and continuous absorption band of oxygen gas at 1.26 and 1.065 mm and radiative lifetime of $^1\Delta_g$ state of oxygen, J. Chem. Phys. 43 (12) (1965) 4345–4350, https://doi.org/10.1063/1.1696694.

[36] J.M. Wessels, M.A.J. Rodgers, Effect of solvent polarizability on the forbidden $^1\Delta_g \rightarrow {}^3\Sigma_g^-$ transition in molecular oxygen: a Fourier transform near-infrared luminescence study, J. Phys. Chem. 99 (1995) 17586–17592.

[37] A.N. Macpherson, T.G. Truscott, Fourier-transform luminescence spectroscopy of solvated singlet oxygen, J. Chem. Soc. Faraday Trans. 90 (8) (1994) 1065–1072.

[38] L. Haley, B. Halperin, J. Koningstein, Electronic Raman transition from an optically pumped excited state, Chem. Phys. Lett. 54 (2) (1978) 389–391, https://doi.org/10.1016/0009-2614(78)80125-0.

[39] P. Myslinski, J.A. Koningstein, Time-resolved excited-state electronic Raman spectrum of ruby, Chem. Phys. Lett. 135 (1–2) (1987) 35–38.

[40] G. Carver, D. Spichiger, P.L.W. Tregenna-Piggott, Electronic Raman spectroscopy of the vanadium (III) hexaaqua cation in guanidinium vanadium sulphate: quintessential manifestation of the dynamical Jahn–Teller effect, J. Chem. Phys. 122 (2005), 124511, https://doi.org/10.1063/1.1872835.

[41] X. Liu, Y. Wang, S. Li, H. Wang, W. Fang, N. Gong, C. Sun, Z. Men, Resonance enhanced cascade stimulated Raman and coherent anti-stokes Raman scattering of symmetric and antisymmetric O-D vibrations, Opt. Commun. 509 (2022), 127861.

[42] Y. Gao, N. Gong, C. Sun, W. Wang, Z. Men, Stimulated Raman scattering investigation of isotopic substitution H_2O/D_2O system, J. Mol. Liq. 297 (2020) 11923.

[43] J.E. Bertie, Z. Lan, Infrared intensities of liquids XX: the intensity of the OH stretching band of liquid water revisited, and the best current values of the optical constants of H_2O(l) at 25°C between 15,000 and 1 cm^{-1}, Appl. Spectrosc. 50 (1996) 1047–1057.

[44] A.N. Macpherson, P.H. Turner, T.G. Truscott, Detection of near-IR singlet oxygen luminescence with an FT-Raman spectrometer, Appl. Spectrosc. 48 (1994) 539–541.

[45] A.A. Krasnovsky Jr., R.V. Ambartzumian, Tetracene oxygenation caused by infrared excitation of molecular oxygen in air-saturated solutions: the photoreaction action spectrum and spectroscopic parameters of the $^1\Delta_g \leftarrow {}^3\Sigma_g^-$ transition in oxygen molecules, Chem. Phys. Lett. 400 (2004) 531–535.

[46] M. Bregbhøj, C.K. Mc Loughlin, T. Breitenbach, P. Ogilby, $X^3\Sigma_g^- \rightarrow b^1\Sigma_g^+$ absorption spectra of molecular oxygen in liquid organic solvents at atmospheric pressure, J. Phys. Chem. A 126 (2022) 3839–3845.

[47] M. Salasi, T. Pojtanabuntoeng, S. Wong, M. Lehmann, Efficacy of bisulfite ions as an oxygen scavenger in monoethylene glycol (at least 20 wt%)/water mixtures, SPE J. 22 (05) (2017) 1467–1477.

[48] R.C. Trivedi, L. Rebar, K. Desal, L.J. Stong, New ultraviolet (340 nm) method for essay of uric acid in serum or plasma, Clin. Chem. 24 (1978) 562–566.

[49] F. Fisher, G. Graschew, H. J. Sinn, W. Maier-Borst, W. J. Lorenz, P. M, Schlag. A chemical dosimeter for the determination of photodynamic activity of photosensitizers, Clin. Chim. Acta, 274 (1998), pp. 89–104.

[50] A.A. Krasnovsky Jr., Photosensitized luminescence of singlet oxygen in solution, Jr. Biofizika 21 (1979) 748–749.

[51] W. Adam, D. Kazakov, V. Kazakov, Singlet-oxygen Chemiluminescence in peroxide reactions, Chem. Rev. 105 (9) (2005) 3371–3387.

[52] R.A. Litjens, T.I. Quickenden, C.G. Freeman, Visible and near-ultraviolet absorption of liquid water, Appl. Opt. 38 (1999) 1216–1223.

[53] E.S. Fry, Visible and near-ultraviolet absorption spectrum of liquid water: comment, Appl. Opt. 39 (16) (2000) 2743–2744.

[54] B. Ozdal, J. Bahram, Demonstration of a silicon Raman laser, Opt. Express 12 (2004) 5269–5273, https://doi.org/10.1038/srep0348410.1364/OPEX.12.005269.

[55] H. Rong, R. Jone, A. Liu, O. Cohen, D. Hak, A. Fang, M. Paniccia, A continuous -wave Raman silicon laser, Nature 433 (2005) 725–728, https://doi.org/10.1038/srep0348410.1038/nature03346.

[56] L. Guo, J. Huang, Y. Chen, B. Zhang, M. Ji, Fiber-enhanced stimulated Raman scattering and sensitive detection of dilute solutions, Biosensors 12 (2022) 243–254.